



Brief paper

Lyapunov-based nonlinear control of nonautonomous systems with individual input constraints[☆]Sai Tej Paruchuri^{a,*}, Andres Pajares^b, Eugenio Schuster^a^a Department of Mechanical Engineering and Mechanics, Lehigh University, Bethlehem, PA 18015, USA^b General Atomics, San Diego, CA 92121, USA

ARTICLE INFO

Article history:

Received 26 April 2023

Received in revised form 27 February 2024

Accepted 3 October 2024

Available online 7 December 2024

Keywords:

Control with input constraints

State-feedback control

Plasma control in tokamaks

ABSTRACT

A control algorithm that can locally stabilize a specific class of multi-input multi-output nonautonomous nonlinear dynamical systems while satisfying individual input constraints is developed. The proposed Lyapunov-based state-feedback control law inherently accounts for the actuator amplitude saturation limits without the need for computationally expensive real-time optimization techniques. In addition to the control law, a formal definition for the local “controllable region” within which the controller can asymptotically drive the system states to the origin and satisfy the input saturation limits is also presented. The nonautonomous nature of the system dynamics implies that the “controllable region” continuously evolves with time. Therefore, a sufficient condition to maintain the system states within the “controllable region” is proposed in this work to make practical implementation feasible. The effectiveness of the controller is tested for a specific control problem arising in tokamaks, which are toroidal devices that use strong magnetic fields to confine a plasma (hot ionized gas). The primary emphasis of tokamak research is to regulate the plasma properties around predetermined values to achieve stable plasma confinement. Nonlinear simulations show that the proposed controller can achieve the desired plasma control objectives in a DIII-D tokamak scenario.

© 2024 Elsevier Ltd. All rights are reserved, including those for text and data mining, AI training, and similar technologies.

1. Introduction

A controller's ability to track an arbitrary set of targets, irrespective of the application, is constrained by the physical saturation limits of the actuators. In some systems, a careful selection of targets may be sufficient to ensure the inputs prescribed by the controller are within the physical saturation limits. However, such flexibility in target selection may not be viable in certain practical applications. In such cases, an unconstrained controller may prescribe inputs that are unrealizable by the physical system. Such physically infeasible inputs can result in undesirable effects, such as the integral windup observed in proportional–integral–derivative (PID) controllers.

A review of existing control literature reveals that several control strategies have been developed to handle the physical constraints on the inputs. The inclusion of anti-windup blocks is one of the most common methods used to handle actuator saturation produced due to integrator windup (Tarbouriech & Turner,

2009). However, the anti-windup prevents saturation a posteriori, i.e., the anti-windup block is separate from the controller block. Furthermore, not all controller algorithms have integral action. Methods like model predictive control (MPC) (Camacho & Alba, 2013) provide a straightforward solution for incorporating actuation constraints into the controller block (Giovannini, 2003; Gutjahr, Gröll, & Werling, 2017; Jeong & Park, 2005; Kapila & Valluri, 1998). During the MPC problem formulation, the actuator saturation limits can be incorporated as algebraic inequality constraints. However, MPC, particularly for nonlinear systems, can be computationally expensive for real-time implementation. Researchers have developed a large class of controllers (both linear and nonlinear) that account for saturation without relying on real-time optimization like MPC. In general, these control strategies for handling saturation constraints can be broadly classified into methods that

- (i) consider bounds on input norms, where the norm of the input vector is bounded by a constant (El-Farra & Christofides, 2003a, 2003b; El-Farra, Mhaskar, & Christofides, 2005; Kose & Jabbari, 2001; Phat & Niamsup, 2015),
- (ii) employ a saturation function, where the unbounded input in the model is replaced by a function of the input that accounts for saturation (Jin, Qin, Shi, & Zheng, 2018; Wang,

[☆] The material in this paper was partially presented at the 2023 American Control Conference (ACC), May 31–June 2, 2023, San Diego, California, USA. This paper was recommended for publication in revised form by Associate Editor Yang Zhu under the direction of Editor Miroslav Krstic.

* Corresponding author.

E-mail addresses: saitejp@lehigh.edu (S.T. Paruchuri), pajares@fusion.gat.com (A. Pajares), schuster@lehigh.edu (E. Schuster).

Chan, & Zhang, 2005; Wang & Liang, 2018; Wu & Grigoriadis, 1999; Yuanyuan, Dayi, & Wenbo, 2021; Zheng, Huang, Xie, & Zhu, 2018),

- (iii) incorporate individual actuator bounds, where the bound on each input is considered (Hu, 2008; Lei, Yu, & Zou, 2008; Leonessa, Haddad, Hayakawa, & Morel, 2009; Nguyen & Jabbari, 2000; Pakmehr & Yucelen, 2014; Piga, Formentin, & Bemporad, 2018; Shen, Xiong, & Hong, 2018; Xiong, Derong, Qinglai, & Ding, 2015).

Most of the literature cited above consider autonomous systems. Solutions for nonautonomous systems (both linear and nonlinear) that account for saturation without relying on real-time optimization like MPC are limited. The explicit dependence of the state and input matrices of linear time-variant systems on time increases the complexity of the problem. Some examples of controllers for linear time-variant systems that incorporate the effect of the input saturation include Niamsup and Phat (2018), Phat and Niamsup (2006). The problem of nonlinear nonautonomous systems with input constraints, as expected, is less explored.

In this work, a Lyapunov-based control algorithm is studied for a certain class of nonlinear nonautonomous systems. A closed-form expression for the control law that intrinsically accounts for the saturation limits is derived. Thus, the presented algorithm does not rely on real-time optimization methods and is computationally inexpensive. A detailed analysis discussing the conditions necessary to prove the closed-loop system's stability and the input's boundedness is presented. The proposed controller is tested by implementing it in a control problem arising in a specific type of plasma-confinement devices (referred to as tokamaks). Nonlinear tokamak-based-plasma-property simulations demonstrate the effectiveness of the controller. The control law presented in this work can be considered as a direct extension of the series of input-bounded control algorithms (based on Sontag's law (Lin & Sontag, 1991)) presented in El-Farra and Christofides (2003a, 2003b), El-Farra et al. (2005) for a particular category of nonlinear autonomous systems. These control algorithms rely on the assumption that the initial condition is contained in a predefined time-invariant "controllable" set. This work generalizes these results on "controllable" sets, input boundedness, and closed-loop stability to a particular class of nonautonomous systems. Since the system is nonautonomous, the "controllable region" is continuously evolving with time. Thus, even if the initial state is contained in the "controllable region", the region can shrink eventually such that the state trajectory is no longer contained in it. Thus, the condition proposed in El-Farra and Christofides (2003a, 2003b), El-Farra et al. (2005) cannot be directly applied to the system under consideration. A new sufficient condition on the system's initial state is presented in this work to handle nonautonomous cases. The "controllable region" definition presented in this work can also be used as an ad hoc definition for controllability for the specific class of systems used in this paper. Controllability is hard, if not impossible, to define for nonlinear systems. The "controllable region" defined in this work can be used to determine the class of trajectories that can be stabilized a priori. Besides, the controllers presented in El-Farra and Christofides (2003a, 2003b), El-Farra et al. (2005) define inputs whose norms are bounded. On the other hand, the control algorithm presented in this work can handle individual input bounds.

The following sections are organized as follows. Section 2 presents the class of nonlinear systems studied in this paper. Section 3 discusses the control law and presents a rigorous stability and input bound analysis. Special cases on how the controller simplifies for autonomous systems and systems with symmetric input bounds are also studied in this section. Section 4 is

reserved for the safety factor profile control problem arising in tokamaks, which are used to confine a plasma (hot ionized gas). The numerical simulation results are given in Section 5. The nonlinear simulations consider a DIII-D tokamak (Fenstermacher et al., 2022) scenario. Finally, the conclusions and potential future extensions of this work are presented in Section 6.

2. Problem formulation

Consider a nonlinear dynamical system governed by ordinary differential equations of the type

$$\dot{\mathbf{x}} = f(\mathbf{x}, t) + g(\mathbf{x}, t)\mathbf{u}(t), \quad \mathbf{x}(0) = \mathbf{x}_0, \quad (1)$$

where $\mathbf{x} \in \mathbb{R}^n$ is the state vector, $\mathbf{u} = [u_1, \dots, u_m]^T \in \mathbb{R}^m$ is the input vector, $f : \mathbb{R}^n \times \mathbb{R}_0^+ \mapsto \mathbb{R}^n$ and $g : \mathbb{R}^n \times \mathbb{R}_0^+ \mapsto \mathbb{R}^{n \times m}$ are nonlinear functions, $\mathbb{R}_0^+ := \mathbb{R}^+ \cup \{0\}$. Suppose the input saturation limits are given by, for each $i \in \{1, \dots, m\}$, for all time t ,

$$\check{u}_i \leq u_i(t) \leq \hat{u}_i. \quad (2)$$

The goal of this work is to develop a computationally inexpensive control algorithm that prescribes the input \mathbf{u} and analyze the conditions under which \mathbf{u} asymptotically stabilizes the system governed by (1) while satisfying the constraints (2). The problem formulated above adheres to the conventional safety factor control problem encountered in tokamaks, as detailed in Section 4.

The following assumptions hold throughout the analysis carried out in the paper.

Assumption 1. The function f satisfies $f(\mathbf{0}, t) + g(\mathbf{0}, t)\mathbf{u}_{off} = \mathbf{0}$, where

$$\mathbf{u}_{off} := \frac{\check{\mathbf{u}} + \hat{\mathbf{u}}}{2}, \quad (3)$$

$\check{\mathbf{u}}, \hat{\mathbf{u}}$ are the vector of lower and upper saturation limits, respectively. In addition, at each time t , any $\mathbf{x} \in \mathbb{R}^n$, the function g satisfies $0 < \underline{g} \leq \|g(\mathbf{x}, t)\| \leq \bar{g}$, where $\|\cdot\|$ represents the induced 2-norm and $\underline{g}, \bar{g} \in \mathbb{R}$ are constants.

In the above assumption, the input \mathbf{u}_{off} can be considered as a feedforward term that offsets the function f . Incorporating the offset term also makes the bounds on the feedback term symmetric. In other words, $\check{u}_i \leq u_i(t) \leq \hat{u}_i \implies -\check{u}_i^* \leq u_i(t) - u_{off,i}(t) \leq \hat{u}_i^*$, where

$$\check{u}_i^* := \left(\frac{\hat{u}_i - \check{u}_i}{2} \right) \geq 0 \quad \text{for } 1 \leq i \leq m. \quad (4)$$

On the other hand, the lower and upper bounds on $|g(\mathbf{x}, t)|$ imply that the influence of the input on the system dynamics neither decreases beyond a certain level nor grows unbounded. Note that the assumption on g can be relaxed by restricting \mathbf{x} to the union over time t of all "controllable regions" (defined in (14)) rather than the entire state space.

Assumption 2. The state $\mathbf{x}(t)$ is contained in the left null space of the matrix $g(\mathbf{x}(t), t)$ only when it is at the origin, i.e., $g(\mathbf{x}(t), t)^T \mathbf{x}(t) = \mathbf{0} \iff \mathbf{x}(t) = \mathbf{0}$.

A direct consequence of the above assumption is that $\|g^T \mathbf{x}\| = 0 \iff \|\mathbf{x}\| = 0$, where $\|\cdot\|$ represents the Euclidean norm of a given vector. The need for these assumptions becomes evident in the theorem proofs presented in Section 3. Analysis on how the above assumptions can be tested for a practical example are presented in Section 5.

3. Control synthesis and analysis

This section presents the control law with the corresponding stability and input bound analysis. In addition, a discussion on how the control law simplifies in certain special cases is also presented.

3.1. Control input definition

The feedback control input that can locally stabilize the system governed by (1) is given by

$$\mathbf{u}(t) = \mathbf{u}_{off} - \mathbf{u}_{tr}(t), \quad (5)$$

where \mathbf{u}_{off} is defined in (3),

$$\mathbf{u}_{tr}(t) = \begin{cases} A(\mathbf{x}(t), t)(s(\mathbf{x}(t), t))^T & \text{if } \|s(\mathbf{x}(t), t)^T\| \neq 0, \\ 0 & \text{if } \|s(\mathbf{x}(t), t)^T\| = 0. \end{cases} \quad (6)$$

The term A in (6) is a diagonal matrix of the form

$$A(\mathbf{x}, t) := \begin{bmatrix} \alpha_1(\mathbf{x}, t) & & 0 \\ & \ddots & \\ 0 & & \alpha_m(\mathbf{x}, t) \end{bmatrix}, \quad (7)$$

where the i th diagonal element is defined as

$$\alpha_i(\mathbf{x}, t) := \frac{r_1(\mathbf{x}, t) + \sqrt{r_2(\mathbf{x}, t)^2 + (\check{u}_i^* \|s(\mathbf{x}, t)^T\|)^4}}{\|s(\mathbf{x}, t)^T\|^2 \left[1 + \sqrt{1 + (\check{u}_i^* \|s(\mathbf{x}, t)^T\|)^2} \right]}. \quad (8)$$

The terms in (6) and (8) are defined as

$$s(\mathbf{x}, t) := \mathbf{x}^T g(\mathbf{x}, t), \quad (9)$$

$$r_1(\mathbf{x}, t) := r(\mathbf{x}, t) + \mu \|2\mathbf{x}\| \left(\frac{\|2\mathbf{x}\|}{\|2\mathbf{x}\| + \lambda} \right), \quad (10)$$

$$r_2(\mathbf{x}, t) := r(\mathbf{x}, t) + \mu \|2\mathbf{x}\|, \quad (11)$$

$$r(\mathbf{x}, t) := \mathbf{x}^T f^*(\mathbf{x}, t), \quad (12)$$

$$f^*(\mathbf{x}, t) := f(\mathbf{x}, t) + g(\mathbf{x}, t)\mathbf{u}_{off}(t), \quad (13)$$

\check{u}_i^* is defined in (4), $\mu > 0$ and $\lambda > 0$ are adjustable scalar parameters. As mentioned in the previous discussions, the control input stabilizes the system locally. From a practical standpoint, it is vital to understand the scope of this local stabilizable region. In this work, a closed-form expression for a set contained in this local stabilizable region is given. This set is termed the ‘‘controllable region’’ in the following analysis and is defined as

$$\Pi_t = \{\mathbf{x} \in \mathbb{R}^n | a(\mathbf{x}, t) \leq b(\mathbf{x}, t)\}, \quad (14)$$

where

$$a(\mathbf{x}, t) := \max\{|r_1(\mathbf{x}, t)|, |r_2(\mathbf{x}, t)|\}, \quad (15)$$

$$b(\mathbf{x}, t) := \check{u}^* \|s(\mathbf{x}, t)^T\|, \quad (16)$$

$$\check{u}^* := \min\{\check{u}_1^*, \dots, \check{u}_m^*\}. \quad (17)$$

Remark 3. The condition in (6) defined in terms of $\|s(\mathbf{x}(t), t)^T\|$ can be replaced by $\|\mathbf{x}(t)\|$ since $\|s(\mathbf{x}(t), t)^T\| = 0 \iff \|\mathbf{x}(t)\| = 0$ (Assumption 2).

Remark 4. The term \check{u}^* , defined in (17), is one of the parameters that determine the size of the ‘‘controllable region’’ Π_t . In certain cases, the size of the set Π_t could be increased by appropriately scaling the input \mathbf{u} , and hence changing the value of \check{u}^* . The Appendix gives a detailed overview of the modified control law with scaled inputs.

3.2. Stability analysis

The following lemma and theorem prove that if the state-feedback input given in (5) is used to close the control loop, then the equilibrium at the origin of the closed-loop system is uniformly asymptotically stable. Recall that the equilibrium at the origin is uniformly asymptotically stable if it is uniformly stable and there is a constant $c > 0$, independent of the initial time t_0 , such that for all $\|\mathbf{x}(t_0)\| < c$, $\mathbf{x}(t) \rightarrow 0$ as $t \rightarrow \infty$ (refer to Chapter 4 of Khalil, 2002). In the following analysis, the explicit dependence of certain terms on the state $\mathbf{x}(t)$ and time t has not been specified for brevity.

Lemma 5. Consider the closed-loop system governed by (1) and (5). If the state \mathbf{x} is contained in the set Π_t at time t , then the time derivative of the Lyapunov function $V = \frac{1}{2}\mathbf{x}^T \mathbf{x}$ is bounded from above by

$$\dot{V} \leq - \frac{\mu \|2\mathbf{x}\|^2}{(\|2\mathbf{x}\| + \lambda) \left[1 + \sqrt{1 + (\check{u}^* \|s^T\|)^2} \right]}, \quad (18)$$

where $\check{u}^* := \max\{\check{u}_1^*, \dots, \check{u}_m^*\}$.

Proof. The time derivative of the Lyapunov function is

$$\dot{V} = \mathbf{x}^T \dot{\mathbf{x}} = \mathbf{x}^T [f + g\mathbf{u}], \quad (19)$$

where (1) is used. From (6), it is clear that the input \mathbf{u} depends on the value of $\|s(\mathbf{x}(t), t)^T\|$. When $\|s(\mathbf{x}(t), t)^T\| = 0$, we have $\mathbf{u} = \mathbf{u}_{off}$. From Assumptions 1 and 2, it is evident that the inequality in (18) holds trivially. On the other hand, if $\|s(\mathbf{x}(t), t)^T\| \neq 0$, we have

$$\dot{V} = \mathbf{x}^T [f^* + g(-As^T)] \quad (20)$$

$$= r + s(-As^T) \quad (21)$$

$$\leq r - \hat{\alpha} \|s^T\|^2, \quad (22)$$

where the equations in (5), (6) and (13) are used. In the above equation, the term $\hat{\alpha}$ is defined as

$$\hat{\alpha} := \min\{\alpha_1, \dots, \alpha_m\}. \quad (23)$$

Suppose the minimum in the above equation is achieved at the j th element, i.e., $\hat{\alpha} = \alpha_j$ with $1 \leq j \leq m$. Let \check{u} be the value of \check{u}_i^* corresponding to the j th actuator, i.e., $\check{u} = \check{u}_j^*$. Using (8), the time derivative of the Lyapunov function can now be written as

$$\begin{aligned} \dot{V} &\leq r - \|s^T\|^2 \left[\frac{r_1 + \sqrt{(r_2)^2 + (\check{u} \|s^T\|)^4}}{\|s^T\|^2 \left[1 + \sqrt{1 + (\check{u} \|s^T\|)^2} \right]} \right] \\ &= \frac{r \left[1 + \sqrt{1 + (\check{u} \|s^T\|)^2} \right] - r_1 - \sqrt{(r_2)^2 + (\check{u} \|s^T\|)^4}}{\left[1 + \sqrt{1 + (\check{u} \|s^T\|)^2} \right]} \\ &\leq \frac{r \left[\sqrt{1 + (\check{u} \|s^T\|)^2} \right] - \sqrt{(r_2)^2 + (\check{u} \|s^T\|)^4}}{\underbrace{\left[1 + \sqrt{1 + (\check{u} \|s^T\|)^2} \right]}_I} \\ &\quad - \frac{\mu \|2\mathbf{x}\|^2}{\underbrace{(\|2\mathbf{x}\| + \lambda) \left[1 + \sqrt{1 + (\check{u}^* \|s^T\|)^2} \right]}_{II}}. \end{aligned} \quad (24)$$

In the above derivation, we have used the fact that $r - r_1 \leq 0$ (refer to (10)) and $\check{\underline{u}} \leq \check{\underline{u}}^*$ (refer to the lemma statement). By hypothesis, the state \mathbf{x} is assumed to be contained in the set Π_t . By definition of Π_t given in (14) and the fact that $\check{\underline{u}}^* \leq \check{\underline{u}}$, we have

$$|r_2| \leq \check{\underline{u}}^* \|s^T\| \leq \check{\underline{u}} \|s^T\|. \quad (25)$$

Thus, at any given time t , the term r_2 can take values in the range $[-\check{\underline{u}} \|s^T\|, \check{\underline{u}} \|s^T\|]$.

Case 1: Suppose that $-\check{\underline{u}} \|s^T\| \leq r_2 \leq 0$. Since the parameter μ in (11) is strictly positive by selection, we conclude that $r \leq 0$. Thus, Term I in (24) is negative, which implies (18).

Case 2: Suppose that $0 < r_2 \leq \check{\underline{u}} \|s^T\|$. Algebraic manipulation will show that

$$-\sqrt{(r_2)^2 + (\check{\underline{u}} \|s^T\|)^4} \leq -r_2 \sqrt{1 + (\check{\underline{u}} \|s^T\|)^2}. \quad (26)$$

Using the above inequality and the fact that r_2 defined in (11) satisfies $r - r_2 \leq 0$, we conclude that Term I in (24) is negative. Hence, we get the inequality in (18).

Theorem 6. *Suppose that the initial condition of the closed-loop system governed by (1) and (5) is such that the state trajectory \mathbf{x} is contained in the set Π_t for all time t . Then, the state \mathbf{x} uniformly converges to the origin as $t \rightarrow \infty$.*

Proof. The Lyapunov analysis carried out in Lemma 5 shows that the time derivative of the Lyapunov function $V = \frac{1}{2} \mathbf{x}^T \mathbf{x}$ is bounded from above by

$$\dot{V} \leq -\frac{\mu \|2\mathbf{x}\|^2}{(\|2\mathbf{x}\| + \lambda) \left[1 + \sqrt{1 + (\check{\underline{u}}^* \|s^T\|)^2} \right]}. \quad (27)$$

Using Cauchy Schwarz inequality, we get

$$\dot{V} \leq -\frac{\mu \|2\mathbf{x}\|^2}{(\|2\mathbf{x}\| + \lambda) \left[1 + \sqrt{1 + (\check{\underline{u}}^* \|g^T\| \|\mathbf{x}\|)^2} \right]}. \quad (28)$$

Using Assumption 1, we conclude that

$$\dot{V} \leq -\frac{\mu \|2\mathbf{x}\|^2}{(\|2\mathbf{x}\| + \lambda) \left[1 + \sqrt{1 + (\check{\underline{u}}^* \bar{g} \|\mathbf{x}\|)^2} \right]}, \quad (29)$$

which is a negative definite function. Using the Lyapunov theorem for nonautonomous systems (Theorem 4.9 in Khalil, 2002), we conclude that the equilibrium at the origin is uniformly asymptotically stable. \square

Remark 7. The above analysis assumes that the model is perfect and u_{tr} is continuous at the origin. If the second assumption does not hold, u_{tr} could be held constant in the neighborhood of the origin such that it is continuous. In such cases and with bounded model uncertainties, it is possible to prove that the state converges to a neighborhood of the origin for certain initial conditions (refer to Chapter 9 of Khalil, 2002).

3.3. Input bound analysis

The input equations shown above include the upper and lower saturation limit values, $\check{\underline{u}}$ and $\check{\underline{u}}$, respectively. However, it is not evident from the input definition if the saturation limits are satisfied at any given time t . The following theorem proves that the control input lies within the saturation bounds (2) provided that the state is contained in the set Π_t .

Theorem 8. *If the state \mathbf{x} of the closed-loop system governed by (1) and (5) is contained in the “controllable region” defined by (14), then the control input $\mathbf{u} = [u_1, \dots, u_m]^T$ defined by (5) satisfies the saturation limits $\check{\underline{u}}_i \leq u_i \leq \check{\underline{u}}_i$ for all $i \in \{1, \dots, m\}$ and all time t .*

Proof. Consider the i th components u_i and $u_{off,i}$ of the input vector \mathbf{u} and \mathbf{u}_{off} , respectively. Since the matrix A is diagonal, (5) and (7) gives us the inequality

$$|u_i - u_{off,i}| \leq |-\alpha_i| |s_i| \quad (30)$$

$$\leq \frac{|r_1 + \sqrt{(r_2)^2 + (\check{\underline{u}}_i^* \|s^T\|)^4}|}{\|s^T\|^2 \left[1 + \sqrt{1 + (\check{\underline{u}}_i^* \|s^T\|)^2} \right]} \|s^T\|. \quad (31)$$

Since the state \mathbf{x} is contained in the set Π_t by hypothesis and since $\check{\underline{u}}^* \leq \check{\underline{u}}_i^*$ by definition in (17), the inequalities

$$|r_1| \leq \check{\underline{u}}^* \|s^T\| \leq \check{\underline{u}}_i^* \|s^T\|, \quad (32)$$

$$|r_2| \leq \check{\underline{u}}^* \|s^T\| \leq \check{\underline{u}}_i^* \|s^T\| \quad (33)$$

hold. Thus, the term $|u_i - u_{off,i}|$ in (30) can further be bounded from above by

$$|u_i - u_{off,i}| \leq \frac{|r_1| + \sqrt{(r_2)^2 + (\check{\underline{u}}_i^* \|s^T\|)^4}}{\|s^T\| \left[1 + \sqrt{1 + (\check{\underline{u}}_i^* \|s^T\|)^2} \right]} \quad (34)$$

$$\leq \frac{\check{\underline{u}}_i^* \|s^T\| + \sqrt{(\check{\underline{u}}_i^* \|s^T\|)^2 + (\check{\underline{u}}_i^* \|s^T\|)^4}}{\|s^T\| \left[1 + \sqrt{1 + (\check{\underline{u}}_i^* \|s^T\|)^2} \right]} \quad (35)$$

$$\leq \frac{\check{\underline{u}}_i^* \|s^T\| \left[1 + \sqrt{1 + (\check{\underline{u}}_i^* \|s^T\|)^2} \right]}{\|s^T\| \left[1 + \sqrt{1 + (\check{\underline{u}}_i^* \|s^T\|)^2} \right]} = \check{\underline{u}}_i^*. \quad (36)$$

Rearranging the terms in the above inequality and using the definition of \mathbf{u}_{off} from (3) proves the theorem. \square

3.4. Sufficient conditions for stability and satisfying input bounds

The theorems in the previous subsection assume that the state \mathbf{x} is contained in the set Π_t at any given time t . Such an assumption might be too strong for practical controller implementation in some real-world applications. In particular, the inherent uncertainty and external disturbance can make it hard to predict the range of values the state \mathbf{x} can take as the closed-loop system evolves. Alternatively, a condition on the initial state \mathbf{x}_0 of the system can make controller implementation more practical. However, even if the initial state \mathbf{x}_0 is contained in the set $\Pi_{t=0}$, the state trajectory can eventually leave the set Π_t . This effect can be attributed to the continuous variation of the “controllable region” with time. Thus, even if the state \mathbf{x} initially converges towards the region, the set Π_t may shrink such that the state is no longer contained in it. No convergence guarantees can be made outside the set Π_t , and thus, the system may become unstable. Fig. 1 gives an intuitive illustration of how shrinking of the set Π_t can result in state divergence from the origin. The following corollaries show that the hypothesis of Theorem 6 can be replaced by conditions on the initial state \mathbf{x}_0 in some instances.

Corollary 9. *Suppose that there exists a ball $B_\varepsilon(\mathbf{0})$ of radius ε centered at the origin contained in the set $\Pi := \bigcap_{t \geq 0} \Pi_t$. The equilibrium at the origin of the closed-loop system is asymptotically stable if the initial condition \mathbf{x}_0 of the system governed by (1) with feedback input (5) is contained in $B_\varepsilon(\mathbf{0})$, i.e., $\mathbf{x}_0 \in B_\varepsilon(\mathbf{0})$.*

Proof. The proof follows directly from the fact that the ball $B_\varepsilon(\mathbf{0}) \subseteq \bigcap_{t \geq 0} \Pi_t$ is invariant since the state \mathbf{x} is always contained in the set Π_t at any given time t . Theorem 6 shows that the closed-loop system is stable. \square

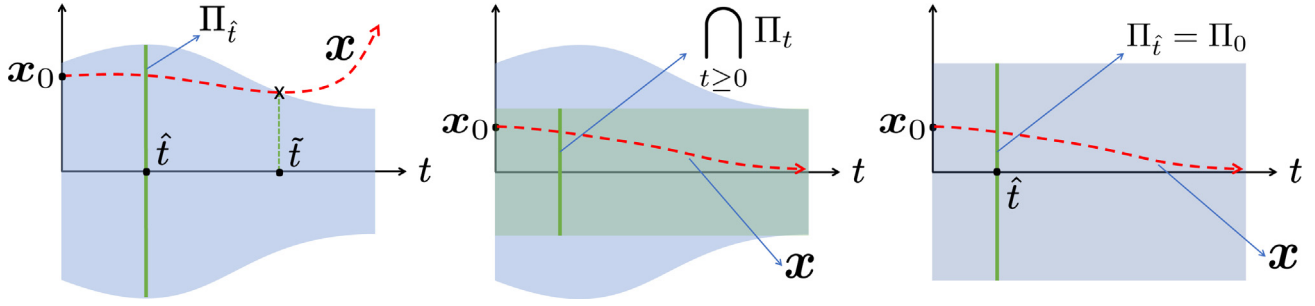


Fig. 1. Controllable regions: Left – Nonautonomous case with initial state contained in $\subseteq \Pi_{t=0}$, Center – Nonautonomous case with initial condition contained in $B_\varepsilon(\mathbf{0}) \subseteq \cap_{t \geq 0} \Pi_t$, Right – Autonomous case with initial state contained in $B_\varepsilon(\mathbf{0}) \subseteq \Pi_{t=0}$.

Corollary 10. Suppose that the nonlinear system governed by (1) is autonomous, i.e., the functions $f(\mathbf{x}, \cdot)$ and $g(\mathbf{x}, \cdot)$ are constant. Furthermore, suppose that the ball $B_\varepsilon(\mathbf{0})$ of radius ε centered at the origin is contained in the set $\Pi_{t=0}$. The equilibrium at the origin is asymptotically stable if the initial condition \mathbf{x}_0 of the closed-loop system (obtained by substituting (5) into (1)) is contained in the ball $B_\varepsilon(\mathbf{0})$.

Proof. Since the functions $f(\mathbf{x}, \cdot)$ and $g(\mathbf{x}, \cdot)$ are constant, the controllable region Π_t does not vary with time. Using an analysis similar to the one used in Corollary 9's proof, we arrive at the required result. \square

A graphical interpretation of both the corollaries discussed above is given in Fig. 1.

4. Application to a tokamak control problem

4.1. Safety factor profile control in tokamaks

The plasma safety factor profile control in tokamaks primarily inspires the control design problem considered in this work. A plasma is a hot ionized gas in which matter exists in the form of positively charged ions and negatively charged electrons. The charged particles in the plasma react to external electric and magnetic fields. A tokamak is a toroidal device that uses strong magnetic fields to confine plasma at high temperatures (about ten times the sun's core temperature) (Wesson & Campbell, 2011). At such high temperatures, the positively charged ions in the plasma can have sufficient kinetic energy to overcome the Coulombic forces of repulsion and fuse together to form heavier nuclei. The difference in masses of the reactants and the products is released as thermal energy. Nuclear fusion research emphasizes maintaining tokamak operating conditions at ideal levels to avoid highly disruptive magnetohydrodynamic instabilities and achieve stable confinement. Ideal operating conditions are prescribed in terms of plasma properties such as safety factor (a parameter related to the pitch of the helical magnetic field) and normalized β (ratio of the kinetic pressure to the magnetic pressure). In fact, MHD studies indicate a direct correlation between these parameters and plasma instabilities. For instance, instabilities called neoclassical tearing modes (NTMs) (Wesson & Campbell, 2011) can arise at locations where the safety factor takes a rational value. Thus, maintaining such plasma parameters at pre-determined optimal conditions is crucial for tokamak operation, and active control may become indispensable.

In this work, the problem of safety factor regulation is considered to demonstrate the effectiveness of the proposed controller. In advanced tokamak (AT) scenarios, the safety factor profile is regulated using noninductive current drives. These are actuators that do not rely on the conventional transformer-like effect to control the plasma parameters. Examples of noninductive drives

used to drive current and heat the plasma include neutral beam injectors or NBIs (which inject a stream of neutrally-charged particles) and electron cyclotron heating and current drives or EC H&CDs (which produce electromagnetic waves whose frequency matches that of the electron cyclotron frequency).

4.2. Finite-dimensional control model

The safety factor is a spatially varying parameter that characterizes the pitch of the helical magnetic field in a tokamak. It is mathematically defined as

$$q(\hat{\rho}, t) := -\frac{B_{\phi,0} \rho_b^2 \hat{\rho}}{\theta(\hat{\rho}, t)}, \quad (37)$$

where $\hat{\rho}$ is the spatial variable and is called the normalized mean effective minor radius, θ is the poloidal flux gradient, ρ_b is the mean effective minor radius of the last closed magnetic flux surface, $B_{\phi,0}$ is the vacuum magnetic field at the magnetic axis. From the above equation, it is evident that the safety factor can be regulated by controlling the poloidal flux gradient θ . The evolution of the poloidal flux gradient is governed by a nonlinear partial differential equation (PDE). Due to the complex nature of the evolution model, the nonlinear PDE is spatially discretized, and the resulting ordinary differential equation (ODE) is used for control synthesis. After using finite-difference approximation, the resulting ODE model takes the form

$$\dot{\theta}(t) = G_\eta(\theta, t)u_\eta + G_{aux}^*(t)\mathbf{P}_{aux} + G_{BS}(\theta, t)u_{BS}, \quad (38)$$

where $\theta \in \mathbb{R}^{N+1}$ is the vector of poloidal flux gradient values at the finite-difference nodes. The terms G_η and G_{BS} are nonlinear functions of the state θ and time t , accounting for the plasma resistivity and bootstrap current (a self-generated current that is driven by the radial pressure gradient in tokamaks) in the poloidal flux gradient model, respectively. The terms u_η and u_{BS} are the virtual inputs that depend on the plasma current, total power and line-averaged electron density. In the context of this work, these terms are assumed to be prescribed values. The term \mathbf{P}_{aux} represents the vector of auxiliary drive powers, comprising neutral beam injector and electron cyclotron heating and current drive powers. It is defined as

$$\mathbf{P}_{aux} = [\mathbf{P}_{NBI}^T, \mathbf{P}_{EC}^T]^T \in \mathbb{R}^m, \quad (39)$$

$$\mathbf{P}_{NBI} = [P_{NBI,1}, \dots, P_{NBI,N_{NBI}}]^T, \quad (40)$$

$$\mathbf{P}_{EC} = [P_{EC,1}, \dots, P_{EC,N_{EC}}]^T, \quad (41)$$

where \mathbf{P}_{NBI} and \mathbf{P}_{EC} are vectors representing the NBI and EC H&CD powers, respectively. The term $G_{aux}^*(t)$ in (38) accounts for the spatial current deposition of the above-mentioned auxiliary drives. In the context of this work, the term \mathbf{P}_{aux} represents the input vector \mathbf{u} that is prescribed by the controller. Note that the total power P_{tot} , which is assumed to be prescribed, depends on the NBI and EC H&CD powers. Thus, as the controller modulates the

NBI and EC H&CD powers, the total power could deviate from the prescribed value. However, it is assumed that additional auxiliary drives, which are tuned for solely heating the plasma without influencing the plasma current or the poloidal flux gradient, are available to compensate for any discrepancies in the total power from the prescribed value. Readers can refer to Pajares and Schuster (2021) for a detailed discussion on the derivation of the above ODE model.

4.3. Error equations

Suppose a target poloidal flux gradient vector $\bar{\theta}$ is given. The evolution of the poloidal flux gradient error $\tilde{\theta} := \theta - \bar{\theta}$ is given by the ODE

$$\dot{\tilde{\theta}}(t) = f(\tilde{\theta}(t), t) + g(t)\mathbf{u}(t) \quad (42)$$

with

$$f(\tilde{\theta}, t) = G_\eta(\theta, t)u_\eta(t) + G_{BS}(\theta, t)u_{BS}(t) - \dot{\tilde{\theta}}, \quad (43)$$

$$g(t) = G_{aux}^*(t), \quad (44)$$

$$\mathbf{u}(t) = \mathbf{P}_{aux}(t). \quad (45)$$

Thus, the goal of the controller is to choose the auxiliary powers $\mathbf{u} = \mathbf{P}_{aux}$ within the saturation limits

$$0 \text{ MW} \leq u_i \leq \bar{P}_i \text{ MW} \quad (46)$$

for all $i \in \{1, \dots, m\}$ to drive the error $\tilde{\theta} \rightarrow 0$ as $t \rightarrow \infty$. Note that \bar{P}_i represents the upper saturation limit of the i th auxiliary drive.

Remark 11. The function f defined above has $\tilde{\theta}$ as one of the variables even though G_η and G_{BS} depend on θ since $\theta = \tilde{\theta} + \bar{\theta}$. Note that the function g does not depend on the state $\tilde{\theta}$, and, as a result, the above model is a special case of the model given in (1). Furthermore, the above definitions of f and g reduce the problem of tracking a target $\bar{\theta}$ to a stabilization problem.

Remark 12. Most tokamak scenarios have a feedforward input component \mathbf{u}_{ff} . In such cases, the feedback input u_{fb} can be calculated as $\mathbf{u}_{fb} := \mathbf{u} - \mathbf{u}_{ff}$, where \mathbf{u} is computed using (5). Such a computation of the feedback input does not require reformulation of the above problem.

Remark 13. For safety factor profile control problem in tokamaks, the error equation (42) and the corresponding ‘‘controllable region’’ Π_t depend on the time evolution of the target $\bar{\theta}$. Generally in tokamak scenarios, the safety factor profile evolves with time. However, during the flat-top phase of certain scenarios, the target can be fixed. In such cases, the target derivative term $\dot{\tilde{\theta}}$ vanishes.

Remark 14. The condition $f^*(\mathbf{0}, t) = 0$ given in Assumption 1 may not hold for all targets $\bar{\theta}$ in (43). However, if the value of $|f^*(\mathbf{0}, t)|$ is small, then, following the discussion in Remark 7, it can be shown that the state converges to a neighborhood of the origin under certain conditions. Note that the simulations discussed in Section 5 demonstrate the effectiveness of the controller while considering a target that does not satisfy the assumption mentioned above.

Remark 15. As noted earlier, a nonlinear partial differential equation governs the poloidal flux gradient in a tokamak, and the model in (38) is obtained using the finite-difference approximation. Since the control law is implemented on an infinite-dimensional system during experiments, it could be valuable

to analyze if the solution of the finite-dimensional closed-loop system approaches its infinite-dimensional counterpart as the number of finite-difference nodes is increased. Using Theorem 3.1 and Remark 3.2 in Verwer and Sanz-Serna (1984), it can be concluded that the convergence of the approximated closed-loop system’s solution to its infinite-dimensional counterpart relies primarily on the Lipschitz continuity of the right-hand side of (42) with respect to the state $\tilde{\theta}$ on a specific set. In particular, the Lipschitz constant must be independent of the grid. Note that the theorems provided in Verwer and Sanz-Serna (1984) assume that the approximation scheme is consistent, and all the solutions to the underlying governing equations are assumed to be unique and sufficiently smooth.

The function f comprises Lipschitz continuous terms, and the existence of a Lipschitz constant independent of the grid is valid. On the other hand, the Lipschitz continuity of the feedback control law (5) could be hard to prove in some tokamak scenarios. The complexity primarily arises from the $\|s(\mathbf{x}, t)^T\|$ term in the denominator of the feedback law, which approaches 0 as the state $\tilde{\theta}$ approaches the origin. To ensure Lipschitz continuity of the input, the value of $\|s(\mathbf{x}, t)^T\|$ could be set to be a small constant when the state enters a neighborhood of the origin. This modification introduces a perturbation term into the closed-loop system’s model. However, as mentioned in Remark 7, the state will converge to a neighborhood of the origin if the perturbation is small.

5. Numerical simulations

The controller developed in Section 3 was tested for a DIII-D tokamak scenario using nonlinear simulations. This section highlights the results of these simulations. During the simulations, 41 finite-difference nodes were considered. The simulations assume that there are 2 NBIs and 1 EC H&CD available for safety factor profile control, i.e., $N_{NBI} = 2$ and $N_{EC} = 1$. In the following description, the notations u_1 and u_2 represent the first and second NBI powers $P_{NBI,1}$ and $P_{NBI,2}$, respectively. The input corresponding to the EC H&CD $P_{EC,1}$ is denoted as u_3 .

The lower bound on three inputs is 0 MW since power cannot be negative. The upper bounds on the 2 NBIs and 1 EC H&CD are 15 MW and 7.5 MW, respectively, i.e., $u_1 \leq 15$ MW, $u_2 \leq 15$ MW, $u_3 \leq 7.5$ MW. Using the formula given in (17), the value of \check{u}_i^* for the three actuators can be calculated as $\check{u}_1^* = 7.5$, $\check{u}_2^* = 7.5$, $\check{u}_3^* = 3.75$. From (14), it is clear the size of the set Π_t depends on $\check{\mathbf{u}}^*$, which is equal to \check{u}_3^* in this case. To increase the size of the ‘‘controllable region’’, the scaling matrix D is selected as $D = \text{diag}(1, 1, 2)$ and the problem is reformulated as discussed in the Appendix. Thus, the size of the scaled controllable region now depends on the minimum of $\check{u}_1 = 7.5$, $\check{u}_2 = 7.5$, $\check{u}_3 = 7.5$.

The effectiveness of the NBIs and EC H&CDs vary with the spatial variable $\hat{\rho}$. The primary reason is that the current deposition profiles of NBIs and EC H&CDs vary with the spatial variable and are typically high for $\hat{\rho} \in [0, 0.5]$. Thus, the controller may not track the target at locations where current deposition is low, i.e., $\hat{\rho} > 0.5$. This is particularly true when the controller cannot prescribe the value of plasma current, which affects the boundary at $\hat{\rho} = 1$. The limited number of actuators and their corresponding saturation limits further restrict the ability of the controller to track the complete target profile. To account for these system limitations, two control nodes at $\hat{\rho} = 0.2$ and $\hat{\rho} = 0.45$. In other words, the controller is designed to track the target at only these two locations. The control inputs are computed using (5) by considering the elements of θ, f , and g that correspond to these two nodes. Note that the simulation model still considers 41 nodes. Thus, the control inputs computed based on the two control nodes are used in the closed-loop simulations

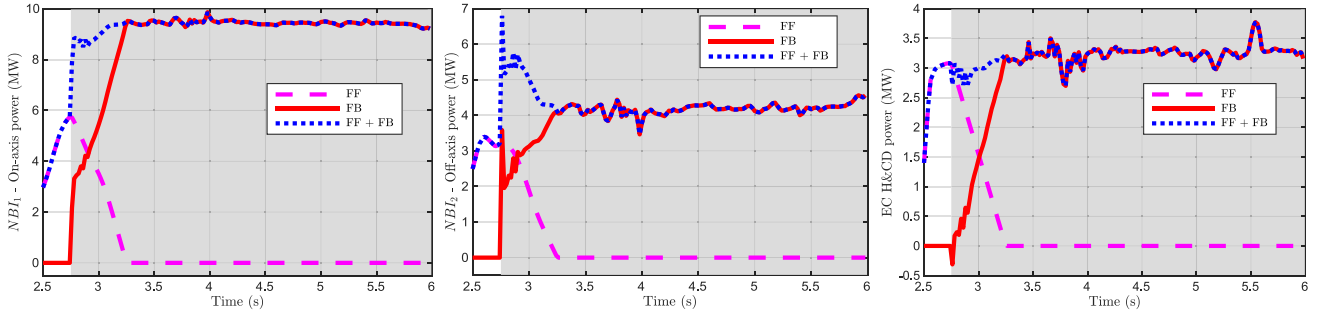


Fig. 2. Auxiliary drive powers: Right – $P_{NBI,1}$ MW, Center – $P_{NBI,2}$ MW, Left – $P_{EC,1}$ MW.

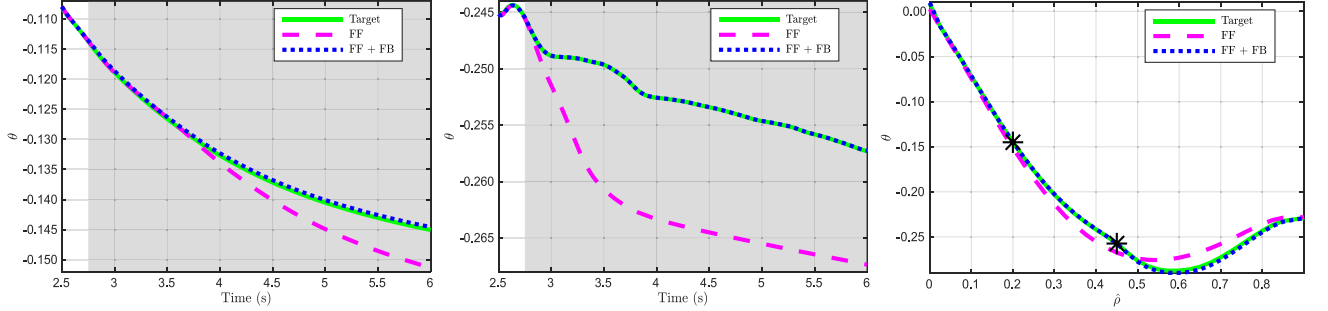


Fig. 3. Poloidal flux gradient: Right – $\theta(0.2, \cdot)$, Center – $\theta(0.45, \cdot)$, Left – $\theta(\cdot, 6s)$.

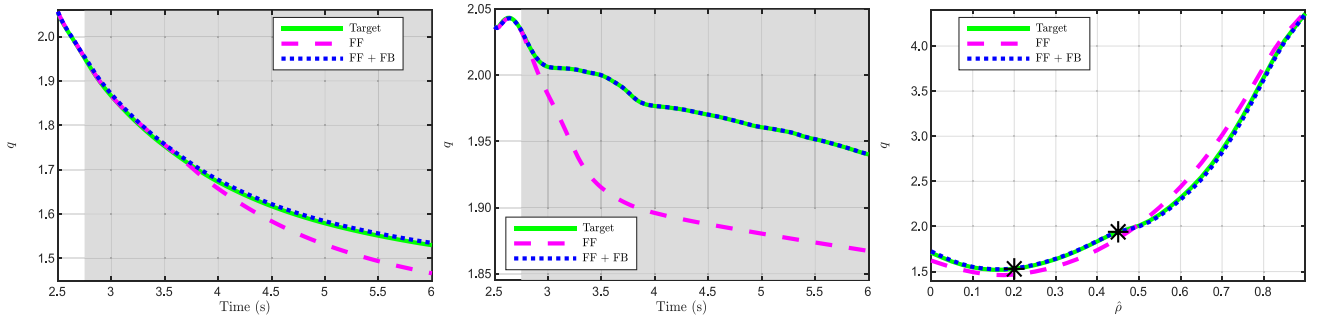


Fig. 4. Safety factor: Right – $q(0.2, \cdot)$, Center – $q(0.45, \cdot)$, Left – $q(\cdot, 6s)$.

of a higher-fidelity model. Furthermore, the control parameters were selected as $\mu = 1 \times 10^{-5}$ and $\lambda = 1$ during the simulations, and the controller was activated at 2.75 s. The gray background denotes the time when the controller is active in all the figures.

Before going over the simulation results, it is crucial to discuss if [Assumptions 1](#) and [2](#) hold for this particular problem formulation. As mentioned in [Remark 14](#), the condition $f^*(\mathbf{0}, t) = 0$ as per [Assumption 1](#) is not precisely satisfied in the simulations. However, as mentioned in the remark, the state should converge close to the target if the value of $f^*(\mathbf{0}, t)$ is small. On the other hand, the bounds on g mentioned in [Assumption 1](#) are trivially valid in almost all tokamak scenarios and are easy to predict a priori. To test the validity of [Assumption 2](#), it is sufficient to show that the dimension of the left null space of g at any given time t is 0. Since two nodes are considered for control with three actuators, the matrix g at any given time t is in $\mathbb{R}^{2 \times 3}$. Since the current deposition profiles of the actuators are different at the two control nodes, the effect of the actuators on the control nodes, characterized by the term $g(t)$ in (44), is different. In other words, the matrix $g(t)$ has independent rows at time t . This implies that the matrix $g(t)$ has rank 2, and its left null space is trivial. Thus, the assumptions necessary for ensuring the closed-loop system's stability and boundedness of the inputs are valid for

the case considered. Note, in case [Assumption 2](#) fails, choosing a different set of control nodes may ensure the validity of the assumption.

[Fig. 2](#) shows the feedback input that was generated by the control algorithm. Generally, for any given target, the feedforward inputs are first computed using techniques such as feedforward optimization. However, in experimental tokamak scenarios, the system uncertainty, and unmodeled dynamics cause the state trajectory to deviate from the target. In the nonlinear simulations, the feedforward inputs shown in [Fig. 2](#) are intentionally selected such that the feedforward trajectory deviates from the target. The feedforward trajectory is then compared to the closed-loop trajectory to examine the effectiveness of the controller. [Fig. 3](#) shows the poloidal flux gradient evolution at the two control nodes. The closed-loop trajectory (denoted $FF + FB$ in the figure) tracks the target as expected. The figure also shows the poloidal flux gradient profile at $t = 6$ s. The profile corresponding to the $FF + FB$ case matches the target profile, thus showing that the choice of control nodes plays a crucial role in determining the error across the whole profile. [Fig. 4](#) shows the safety factor evolution at the two control nodes and the safety factor profile at $t = 6$ s. The safety factor results conclude that the controller effectively achieves the desired control objective. In addition to

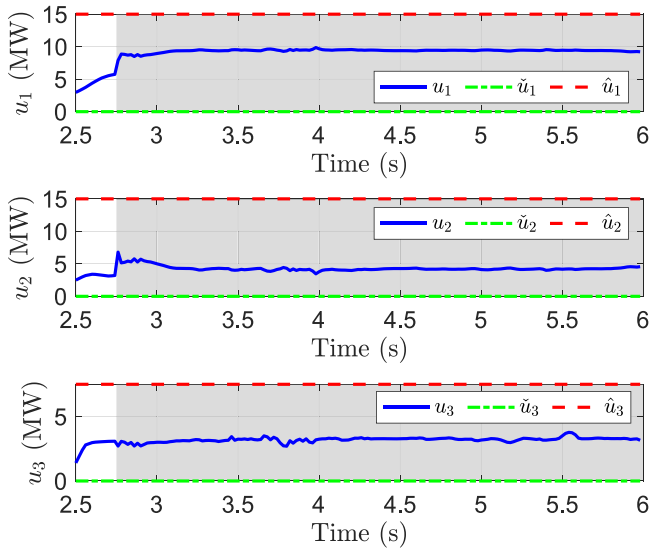


Fig. 5. Input values with upper and lower bounds.

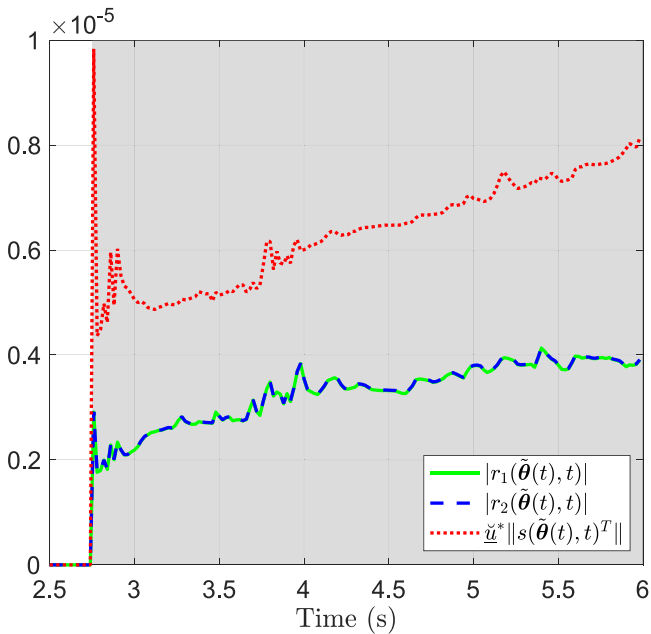


Fig. 6. Hypothesis testing.

asymptotically stabilizing the system, another primary objective of the controller is to ensure that the inputs agree with the saturation limits. Fig. 5 clearly shows that the inputs agree with the upper and lower bounds. Fig. 6 shows that the closed-loop system's state is contained in the set Π_t during the simulation.

6. Conclusion

A Lyapunov-based state-feedback control law that implicitly accounts for the actuator saturation limits is developed in this work. The assumptions made on the system and the hypothesis required for asymptotically stabilizing the system and maintaining the input within the saturation limits are discussed rigorously. Sufficient conditions are developed to make the practical implementation of the controller feasible for a certain class of real-world systems. This work also addresses how the controller can be implemented to regulate the safety factor profile in a tokamak.

Nonlinear simulations carried out for a DIII-D tokamak scenario are presented in this work. The simulation results illustrate the effectiveness of the controller in achieving the desired control objective. Future extensions of this work can potentially include testing the controller in higher-fidelity models, implementing the controller for simultaneous regulation of multiple plasma profiles, and experimental validation of the controller performance.

Acknowledgments

This material is based upon work supported by the U.S. Department of Energy, Office of Science, Office of Fusion Energy Sciences, under Award Numbers DE-SC0010661, DE-SC0021385 and DE-FC02-04ER54698. *Disclaimer:* This report was prepared as an account of work sponsored by an agency of the United States Government. Neither the United States Government nor any agency thereof, nor any of their employees, makes any warranty, express or implied, or assumes any legal liability or responsibility for the accuracy, completeness, or usefulness of any information, apparatus, product, or process disclosed, or represents that its use would not infringe privately owned rights. Reference herein to any specific commercial product, process, or service by trade name, trademark, manufacturer, or otherwise does not necessarily constitute or imply its endorsement, recommendation, or favoring by the United States Government or any agency thereof. The views and opinions of authors expressed herein do not necessarily state or reflect those of the United States Government or any agency thereof.

Appendix. Input scaled control law

As mentioned in Remark 4, the size of the set Π_t depends on the minimum value of $\check{u}_i^* := (\hat{u}_i - \check{u}_i)/2$ for $i = 1, \dots, m$. The inputs can be scaled such that the value \check{u}_i^* corresponding to each of the inputs are equal. The scaling of the input \mathbf{u} is achieved by defining $\hat{\mathbf{u}} := D\mathbf{u}$, where $\hat{\mathbf{u}}$ is the new input vector such that $\check{u}_i^* = \check{u}_i^*$ for all i . The term D is a diagonal scaling matrix of the form

$$D = \text{diag}(d_1, \dots, d_m), \quad (\text{A.1})$$

where $d_i > 0$ for $i = 1, \dots, m$. A new function $\hat{g} := gD^{-1}$ replaces g in the governing equation (1) to account for the scaling of the inputs. This is evident from the fact $\hat{g}\hat{\mathbf{u}} = gD^{-1}D\mathbf{u} = g\mathbf{u}$. The governing equations can be rewritten as

$$\dot{\mathbf{x}} = f(\mathbf{x}, t) + \hat{g}(\mathbf{x}, t)\hat{\mathbf{u}}(t), \quad (\text{A.2})$$

where $\hat{\mathbf{u}} = [\hat{u}_1, \dots, \hat{u}_m]^T \in \mathbb{R}^m$ is the scaled input vector. Note that the lower and upper saturation limits of the new input $\hat{\mathbf{u}}$ are given by $\check{u}_i := d_i\check{u}_i$ and $\hat{u}_i := d_i\hat{u}_i$ for $i = 1, \dots, m$, respectively. The new control law for stabilizing (A.2) can be synthesized using the steps presented in Section 3.

References

- Camacho, Eduardo F., & Alba, Carlos Bordons (2013). *Model predictive control*. Springer science & business media.
- El-Farra, Nael H., & Christofides, Panagiotis D. (2003a). Bounded robust control of constrained multivariable nonlinear processes. *Chemical Engineering Science*, 58(13), 3025–3047.
- El-Farra, Nael H., & Christofides, Panagiotis D. (2003b). Coordinating feedback and switching for control of hybrid nonlinear processes. *AIChE Journal*, 49(8), 2079–2098.
- El-Farra, Nael H., Mhaskar, Prashant, & Christofides, Panagiotis D. (2005). Output feedback control of switched nonlinear systems using multiple Lyapunov functions. *Systems & Control Letters*, 54(12), 1163–1182.
- Fenstermacher, M. E., et al. (2022). DIII-D research advancing the physics basis for optimizing the tokamak approach to fusion energy. *Nuclear Fusion*, 62(4), Article 042024.

Giovanini, Leonardo L. (2003). Model predictive control with amplitude and rate actuator saturation. *ISA Transactions*, 42(2), 227–240.

Gutjahr, B., Gröll, L., & Werling, M. (2017). Lateral Vehicle Trajectory Optimization Using Constrained Linear Time-Varying MPC. *IEEE Transactions on Intelligent Transportation Systems*, 18(6), 1586–1595.

Hu, Qinglei (2008). Robust adaptive sliding mode attitude maneuvering and vibration damping of three-axis-stabilized flexible spacecraft with actuator saturation limits. *Nonlinear Dynamics*, 55(4), 301.

Jeong, Seung Cheol, & Park, PooGyeon (2005). Constrained MPC algorithm for uncertain time-varying systems with state-delay. *IEEE Transactions on Automatic Control*, 50(2), 257–263.

Jin, X., Qin, J., Shi, Y., & Zheng, W. X. (2018). Auxiliary fault tolerant control with actuator amplitude saturation and limited rate. *IEEE Transactions on Systems, Man, and Cybernetics: Systems*, 48(10), 1816–1825.

Kapila, V., & Valluri, S. (1998). Model predictive control of systems with actuator amplitude and rate saturation. In *Proceedings of the 37th IEEE conference on decision and control (cat. no.98CH36171)*, vol. 2 (pp. 1396–1401).

Khalil, Hassan K. (2002). *Nonlinear systems* (3rd ed.). Pearson.

Kose, I. E., & Jabbari, F. (2001). Control of systems with actuator amplitude and rate constraints. In *Proceedings of the 2001 American control conference (cat. no.01CH37148)*, vol. 6 (pp. 4914–4919).

Lei, J., Yu, H., & Zou, H. (2008). Design of an intelligent global terminal backstepping controller without derivative for a class of input constrained high-supersonic missiles. In *2008 international conference on computer science and software engineering*, vol. 1 (pp. 395–398).

Leonessa, Alexander, Haddad, Wassim M., Hayakawa, Tomohisa, & Morel, Yannick (2009). Adaptive control for nonlinear uncertain systems with actuator amplitude and rate saturation constraints. *International Journal of Adaptive Control and Signal Processing*, 23(1), 73–96.

Lin, Yuandan, & Sontag, Eduardo D. (1991). A universal formula for stabilization with bounded controls. *Systems & Control Letters*, 16(6), 393–397.

Nguyen, T., & Jabbari, F. (2000). Output feedback controllers for disturbance attenuation with actuator amplitude and rate saturation. *Automatica*, 36(9), 1339–1346.

Niamsup, Piyapong, & Phat, Vu N. (2018). Robust finite-time H_∞ control of linear time-varying delay systems with bounded control via Riccati equations. *International Journal of Automation and Computing*, 15(3), 355–363.

Pajares, Andres, & Schuster, Eugenio (2021). Current profile and normalized beta control via feedback linearization and Lyapunov techniques. *Nuclear Fusion*, 21.

Pakmehr, M., & Yucelen, T. (2014). Adaptive control of uncertain systems with gain scheduled reference models and constrained control inputs. In *2014 American control conference (pp. 691–696)*.

Phat, V. N., & Niamsup, P. (2006). Stabilization of linear nonautonomous systems with norm-bounded controls. *Journal of Optimization Theory and Applications*, 131(1), 135–149.

Phat, V. N., & Niamsup, P. (2015). Global stabilization of linear time-varying delay systems with bounded controls. *Applied Mathematics Letters*, 46, 11–16.

Piga, D., Formentin, S., & Bemporad, A. (2018). Direct data-driven control of constrained systems. *IEEE Transactions on Control Systems Technology*, 26(4), 1422–1429.

Shen, X., Xiong, Z., & Hong, Y. (2018). Point-to-Point Iterative Learning Control Based on Updating Reference Trajectory with Constrained Input. In *2018 IEEE 7th data driven control and learning systems conference (pp. 788–793)*.

Tarbouriech, Sophie, & Turner, Matthew (2009). Anti-windup design: An overview of some recent advances and open problems. *IET Control Theory & Applications*, 3(1), 1–19.

Verwer, J. G., & Sanz-Serna, J. M. (1984). Convergence of method of lines approximations to partial differential equations. *Computing*, 33(3), 297–313.

Wang, Jin-Zhi, Chan, C. W., & Zhang, Ji-Feng (2005). Global stability of systems with amplitude and rate saturation compensation. *International Journal of Robust and Nonlinear Control*, 15(4), 155–170.

Wang, C., & Liang, M. (2018). Adaptive NN tracking control for nonlinear fractional order systems with uncertainty and input saturation. *IEEE Access*, 6, 70035–70044.

Wesson, John, & Campbell, David J. (2011). *Tokamaks: vol. 149*, Oxford University Press.

Wu, Fen, & Grigoriadis, K. M. (1999). LPV-based control of systems with amplitude and rate actuator saturation constraints. In *Proceedings of the 1999 American control conference (cat. no. 99CH36251)*, vol. 5 (pp. 3191–3195).

Xiong, Y., Derong, L., Qinglai, W., & Ding, W. (2015). Adaptive dynamic programming for H_∞ control of constrained-input nonlinear systems. In *2015 34th Chinese control conference (pp. 3027–3032)*.

Yuanyuan, T., Dayi, W., & Wenbo, L. (2021). Reconfigurability evaluation method for input-constrained control systems. *Journal of Systems Engineering and Electronics*, 32(5), 1023–1030.

Zheng, Z., Huang, Y., Xie, L., & Zhu, B. (2018). Adaptive trajectory tracking control of a fully actuated surface vessel with asymmetrically constrained input and output. *IEEE Transactions on Control Systems Technology*, 26(5), 1851–1859.



Sai Tej Paruchuri is a research scientist in the Department of Mechanical Engineering and Mechanics at Lehigh University, Bethlehem, PA, USA. He earned a B.E. in Mechanical Engineering from Thiagarajar College of Engineering, Anna University, Madurai, India, followed by an M.S. in Mathematics and a Ph.D. in Mechanical Engineering from Virginia Tech, Blacksburg, VA, USA. His research interests encompass nonlinear control, adaptive function estimation and control, reproducing kernel Hilbert spaces, data-driven modeling and control, and reinforcement learning. Currently, his research is primarily aimed at addressing control challenges in nuclear fusion and tokamaks.



Andres Pajares obtained his M.Sc. degree in Aerospace Engineering from the University of Seville (2012) and his Ph.D. in Mechanical Engineering from Lehigh University (2019). Dr. Pajares is currently a research scientist within the Plasma Control and Operations group of General Atomics. His work focuses on the development and experimental testing of plasma-control algorithms at the DIII-D National Fusion Facility in San Diego, where he is stationed, as well as for NSTX-U and ITER. His research interests include physics-based plasma modeling, magnetic control, density control, profile control, and the design of integrated algorithms for plasma-control applications.



Eugenio Schuster received a B.Sc./M.Sc. degree in Electronic Engineering from the University of Buenos Aires, a B.Sc./M.Sc. degree in Nuclear Engineering from the Balseiro Institute, and a Ph.D. degree in Aerospace Engineering from the University of California at San Diego. He is currently a Professor with the Department of Mechanical Engineering and Mechanics, Lehigh University, Bethlehem, PA, USA. He is an expert in nuclear-fusion plasma control and leads the Lehigh University Plasma Control Laboratory. He was a recipient of the National Science Foundation (NSF) CAREER Award for his work on “Nonlinear Control of Plasmas in Nuclear Fusion.” Prof. Schuster has been appointed as a Scientist Fellow in Plasma Control by the ITER Organization. Moreover, he has been designated by the U.S. Department of Energy (DOE) as an expert member of the Integrated Operation Scenarios (IOS) Topical Group within the International Tokamak Physics Activity (ITPA), which he is currently chairing. He has served as Leader of the Operations and Control Topical Group within the U.S. Burning Plasma Organization (BPO) and as founder chair of the Technical Committee on Power Generation within the IEEE Control Systems Society.